Journal of Nuclear Materials 402 (2010) 15–24

Contents lists available at ScienceDirect

Journal of Nuclear Materials

journal homepage: www.elsevier.com/locate/jnucmat

Thermodynamic assessment of the U–Mo–Al system

X. Zhang [a], Y.F. Cui [a], G.L. Xu [a], W.J. Zhu [a], H.S. Liu [a,b,*], B.Y. Yin [c], Z.P. Jin [a,b]

[a] School of Materials Science and Engineering, Central South University, Changsha, Hunan 410083, PR China
[b] Center of Phase Diagrams and Materials Design, Central South University, Changsha, Hunan 410083, PR China
[c] China Institute of Atomic Energy, Beijing 102413, PR China

ARTICLE INFO

Article history:
Received 22 December 2009
Accepted 19 April 2010

ABSTRACT

Thermodynamic assessment of the U–Mo–Al ternary system has been performed by CALPHAD method. Firstly, the U–Mo binary system has been thermodynamically optimized. The reported five solution phases, liquid, orthorhombic_A20 (αU), tetragonal_U (βU), BCC_A2 (γU) and terminal Mo solid solution are treated as substitutional solution phases. The BCC_A2 takes the same structure as Mo thus they are described with the same model. And the only intermetallic compound, MoU_2, is treated as stoichiometric compound. Secondly, by using the available thermodynamic parameters of the Al–U and Al–Mo binary systems reported in literatures, the U–Mo–Al ternary system was thermodynamically assessed. A set of self-consistent thermodynamic parameters has been obtained, which can satisfactorily reproduce most of the thermodynamic and phase diagram data.

1. Introduction

Many research reactors have been operated with highly enriched metal alloy fuel since many decades. However, the fuel with highly enriched uranium has the risk of nuclear proliferation [1]. So since 1978, the Reduced Enrichment for Research Test Reactors (RERTR) program had required to use low-enriched uranium (LEU) instead of high-enriched uranium (HEU) in order to minimize this proliferation risks [2–4], which need a large increase of uranium per unit volume to compensate for the reduction in enrichment. It was confirmed that the uranium silicide dispersion fuels such as U_3Si_2/Al had a relatively high uranium density of 4.8 g-U cm^{-3} as well as the better irradiation stability, which still could not satisfy the design requirements of the more advanced research reactor [5].

Therefore, through the technical study and the reactor irradiation experiments, it is found that the U–Mo alloy is the promising uranium alloy for a high uranium density dispersion fuel due to the large solubility of Mo in γ-U has fine irradiation properties for reactor fuels [2,6–9], and its core uranium density can be 8–9 g-U cm^{-3} [5]. Hence it has become the focus of the fuel development in the RERTR program. The reactor fuel consists of atomized U–Mo particles dispersed in an aluminum matrix. As a result, reaction of U–Mo alloy with the Al matrix may proceed by interdiffusion. Such reaction may affect the performance of nuclear fuel materials. So it is of key importance to understand the U–Mo binary and U–Mo–Al ternary phase diagrams and their thermodynamic properties for the research and development of a UMo-based LEU fuel, behaving in a satisfactory manner under irradiation.

However, the phase diagram of the U–Mo binary system has not been optimized since Massalski [10] established an experimental one based on previous investigations. And thermodynamic assessment of the U–Mo–Al ternary system has not been reported either. This work aims at optimizing the U–Mo–Al ternary system by CALPHAD approach [11].

2. Evaluation of experimental information

A summary of the crystal information of all phases in the U–Mo–Al ternary system is listed in Table 1.

2.1. The U–Mo binary system

The phase diagram of the U–Mo binary system up to 19 wt.% Mo below 1173 K was determined with X-ray Diffraction (XRD), metallographic method as well as chemical analysis by Dwight [12]. It was reported that a eutectoid reaction BCC_A2 $\Longleftrightarrow$ MoU_2 + ort_A20 occurred at 838 K with l0.5 wt% Mo, and the eutectoid reaction tetr_U $\Longleftrightarrow$ BCC_A2 + ort_A20 was located at 912 K with the limit of the tetr_U + BCC_A2 two phase field at 4.5 wt.% Mo. Later, Ackermann and Garg [13] measured the liquidus from 30.4 to 57.6 at.% Mo and the solidus of the BCC_A2 phase by adopting optical technique. The temperature and composition of the peritectic reaction among liquid, Mo and BCC_A2 were studied by Ackermann and Garg [13], Hansen and Anderko [14]. However, the data in Ref. [13] may be considered more reliable than the reported data [14], for the experimental deviations of the latter ones are comparatively large.

* Corresponding author.
E-mail address: hsliu@mail.csu.edu.cn (H.S. Liu).

0022-3115/$ - see front matter © 2010 Elsevier B.V. All rights reserved.
doi:10.1016/j.jnucmat.2010.04.018

Table 1
Crystal information of U–Mo–Al system.[a]

Phase	Crystal system	Pearson symbol	Space group	Strukturbericht designation	Prototype
(αU)	Orthorhombic	*oC4*	*Cmcm*	*A20*	αU
(βU)	Tetragonal	*tP30*	$P4_2/mnm$	A_b	βU
(γU)	Cubic	*cI2*	$Im\bar{3}m$	*A2*	W
(Mo)	Cubic	*cI2*	$Im\bar{3}m$	*A2*	W
(Al)	Cubic	*cF4*	$Fm\bar{3}m$	*A1*	Cu
MoU_2	Tetragonal	*tI6*	*I4/mmm*	$C11_b$	$MoSi_2$
UAl_4	Orthorhombic	*oI20*	*Imma*	$D1_b$	UAl_4
UAl_3	Cubic	*cP4*	$Pm\bar{3}m$	$L1_2$	$AuCu_3$
UAl_2	Cubic	*cF24*	$Fd\bar{3}m$	*C15*	$MgCu_2$
$Al_{12}Mo$	Cubic	*cI26*	$Im\bar{3}$	–	$Al_{12}W$
Al_5Mo	Hexagonal	*hP12*	$P6_3$	–	Al_5W
$Al_{22}Mo_5$	Orthorhombic	*oF216*	*Fdd2*	–	$Al_{22}Mo_5$
$Al_{17}Mo_4$	Monoclinic	*mC84*	*C2*	–	$Al_{17}Mo_4$
Al_4Mo	Monoclinic	*mC30*	*Cm*	–	Al_4W
Al_3Mo	Monoclinic	*mC32*	*Cm*	–	Al_3Mo
Al_8Mo_3	Monoclinic	*mC22*	*C2/m*	–	Al_8Mo_3
$Al_{63}Mo_{37}$	–	–	–	–	–
AlMo	Cubic	*cI2*	$Im\bar{3}m$	*A2*	W
$AlMo_3$	Cubic	*cP8*	$Pm\bar{3}n$	*A15*	Cr_3Si
UMo_2Al_{20}	Cubic	*cF184*	$Fd\bar{3}m$	–	$CeCr_2Al_{20}$
$U_6Mo_4Al_{43}$	Hexagonal	*hP106*	$P6_3/mcm$	–	$Ho_6Mo_4Al_{43}$
$UAl_{2-x}Mo_x$	Hexagonal	*hP12*	$P6_3/mmc$	*C14*	$MgZn_2$

[a] To facilitate reading and writing, some symbols are given here to denote the respective prototype structures as: ort_A20 stands for αU, tetr_U for βU, BCC_A2 for γU and FCC_A1 for Al solid solution.

The diagram established by Brewer et al. [15] indicates that the intermetallic compound MoU_2 congruently transforms into BCC_A2 at around 875 K. Besides, the eutectoid reaction BCC_A2 $\Longleftrightarrow MoU_2 + Mo$ also exists in the U–Mo system [10]. In the light of Massalski [10], the temperature of this reaction is 853 K, which is adopted in the present work.

As for thermodynamic data, Saroja et al. [16] have calculated the excess relative partial molar enthalpy of liquid of U–Mo system from 1550 K to 2280 K by applying the measured liquidus data [13] and the reported free energy of fusion [17]. Parida et al. [6] measured the enthalpy increment of the metastable γ-$U_{0.823}Mo_{0.177}$ in the temperature range 299.0–820.6 K and calculated the enthalpy of formation of the metastable γ-$U_{0.823}Mo_{0.177}$. Then the enthalpy and the heat capacity of the metastable γ-$U_{0.823}Mo_{0.177}$ phase could be obtained from the measured data.

2.2. The Al–Mo and U–Al binary systems

The Al–Mo binary system has been assessed by Saunders [18]. According to the assessed phase diagram [18], only three stoichiometric compounds, $Al_{12}Mo$, Al_5Mo, and Al_4Mo between Al and Al_8Mo_3 were considered, which was in contradiction with the phase diagram presented by Schuster et al. [19] and the version re-evaluated by Eumann et al. [20] later. Recently, Du et al. [21]

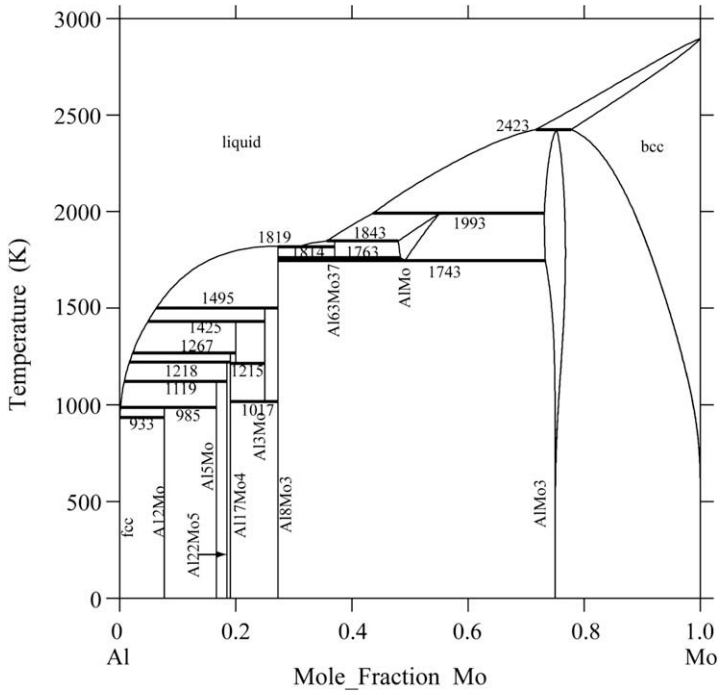

Fig. 1. The Al–Mo binary system assessed by Du et al. [21].

re-assessed the Al–Mo binary system, and satisfactorily reproduced most experimental phase diagram and thermodynamic properties. Hence, the parameters assessed by Du et al. [21] were directly adopted in present work, with which the optimized diagram of Al–Mo system is calculated as is shown in Fig. 1.

The U–Al phase diagram was first assessed by Kassner et al. [22]. However, some uncertain parts exist in their phase diagram. So, Wang et al. [23] re-assessed the phase diagram of the U–Al binary system and good agreement between experiments and assessment has been obtained. However it was found by Tougait and Noël [24] that the compound UAl_4 forms as fully stoichiometric compound without constitutional defect in the U sublattice. Therefore, the α-Al_4U to β-Al_4U transformation does no longer exist. So in this work the compound UAl_4 is treated as stoichiometric compound. With minor modification, the assessed version (Fig. 2) by Wang et al. [23] was adopted in present work.

2.3. The U–Mo–Al ternary system

Phase relations in the U–Mo–Al ternary system were experimentally investigated. Noël et al. [25] experimentally studied the isothermal sections at 673 K and 1073 K [25]. According to Noël et al. [25], three ternary compounds were discovered: $UMo_{2-x}Al_{20+x}$ ($-0.3 < x < 0.75$ at 1073 K) with the cubic structure $CeCr_2Al_{20}$ (space group Fd3 m), $U_6Mo_{4+x}Al_{43-x}$ ($0 < x < 3$ at 1073 K) with the hexagonal $Ho_6Mo_4Al_{43}$ structure (space group $P6_3/mcm$), and $UAl_{2-x}Mo_x$ ($0.6 < x < 0.7$ at 1073 K, $0.7 < x < 0.85$ at 673 K), a laves phase of hexagonal $MgZn_2$ type. The hexagonal-$U_6Mo_4Al_{43}$ and diamond cubic-UMo_2Al_{20}, were later confirmed to exist in the alloys with composition 85.7Al–11.44U–2.86Mo and 87.5Al–10U–2.5Mo in at.% homogenized at 773 K for 200 h by adopting X-ray diffraction, SEM and TEM/STEM method [26].

Besides, as indicated by Noël et al. [25], the substitution of Al by Mo atoms in the cubic ($MgCu_2$ type) binary UAl_2 phase leads to a remarkable solid solution $UAl_{2-x}Mo_x$ up to $x = 0.5$, rather than the substitution of Mo atoms to U sites, leading to $(U,Mo)Al_x$ proposed by Keiser et al. [27].

The liquid equilibria in the U-UAl_2-Al_8Mo_3-Mo system were determined by Petzow and Rexer [28] using DTA, chemical analysis, X-ray diffraction as well as optical microscopy. Afterwards a revised version of liquidus projection was reported by Alekseeva and Korniyenko [29] based on the Petzow's data, with modifications to ensure compatibility the accepted boundary binary systems. Both of the two diagrams excluded the Al-rich part, so many phase relations and reactions are in need of further study.

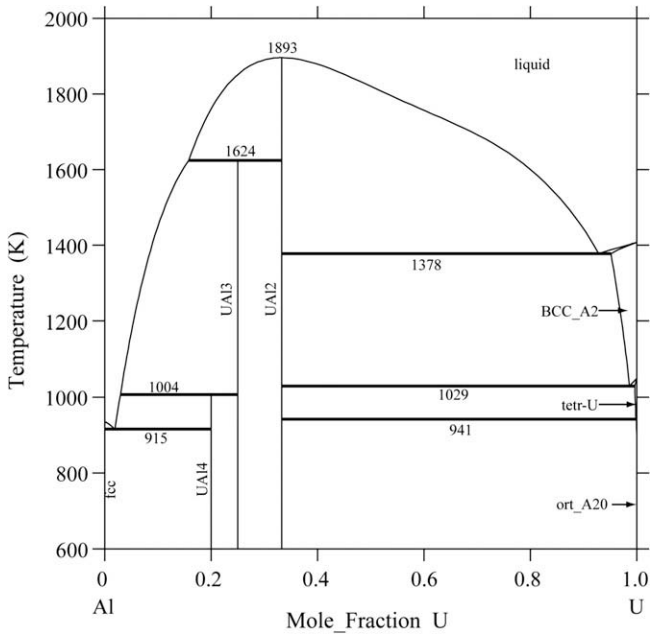

Fig. 2. The U–Al binary system assessed by Wang et al. [23] with minor modification.

3. Thermodynamic models

Different models are employed to describe the solution phases and intermetallic compounds in the U–Mo–Al ternary system.

3.1. Pure elements

The mole Gibbs energy of a pure element i in a status Φ is written referred to the enthalpy of its stable state at $T = 298.15$ K and $P = 101325$ Pa:

$$ {}^0G_i^{\phi} - H_i^{SER} = a + bT + cT\ln T + \cdots \tag{1} $$

which is also called lattice stability, most of which can be cited from Dinsdale [30]. The ${}^0G_{Mo}^{\alpha-U}$ and the ${}^0G_{Mo}^{\beta-U}$ are expressed as follows:

$$ {}^0G_{Mo}^{ort\_A20} = {}^0G_{Mo}^{BCC} + A \tag{2} $$

$$ {}^0G_{Mo}^{tetr\_U} = {}^0G_{Mo}^{BCC} + B \tag{3} $$

where the A and B are parameters to be optimized.

3.2. Solution phases

A substitutional solution model based on random mixing of the constituent atoms is employed to describe the solution phases including liquid, ort_A20, tetr_U, BCC_A2, and FCC_A1 phase. The molar Gibbs energy of a solution phase Φ (Φ = liquid, ort_A20, tetr_U, BCC_A2, FCC_A1,) can be represented as the sum of the weighted Gibbs energy for the pure components, the ideal entropy term describing a random mixing of the components, and the excess Gibbs energy describing the degree of deviation from ideal mixing, i.e.

$$ G_m^{\Phi} = \sum_{i=Al,Mo,U} x_i {}^0G_i^{\Phi} + RT \sum_{i=Al,Mo,U} x_i \ln x_i + {}^EG_m^{\Phi} \tag{4} $$

where G_m^{Φ} is the molar Gibbs energy of a solution phase Φ, ${}^0G_i^{\Phi}$ the Gibbs energy of pure element i (i = Al, Mo, U) in the structural state of Φ, R the gas constant, and T temperature. And the excess Gibbs energy, ${}^EG_m^{\Phi}$, can be expressed by the Redlich–Kister polynomial function as follows:

$$ \begin{aligned} {}^EG_m^{\Phi} = {} & x_{Mo}x_U \sum_{j=0,1\ldots}^{n} {}^{(j)}L_{Mo,U}^{\Phi}(x_{Mo} - x_U)^j + x_{Al}x_U \sum_{j=0,1\ldots}^{n} {}^{(j)}L_{Al,U}^{\Phi}(x_{Al} - x_U)^j \\ & + x_{Al}x_{Mo} \sum_{j=0,1\ldots}^{n} {}^{(j)}L_{Al,Mo}^{\Phi}(x_{Al} - x_{Mo})^j + x_{Al}x_{Mo}x_U L_{Al,Mo,U}^{\Phi} \end{aligned} \tag{5} $$

where x_U, x_{Mo} and x_{Al} are the mole fractions of component U, Mo and Al respectively. ${}^{(j)}L_{Al,Mo}^{\Phi}$ and ${}^{(j)}L_{Al,U}^{\Phi}$ are respectively taken from Du et al. [21] and Wang et al. [23], and ${}^{(j)}L_{Mo,U}^{\Phi}$ is the interaction parameter between Mo and U that can be temperature dependent, and is formulated as:

$$ {}^{(j)}L_{Mo,U}^{\Phi} = A_j + B_jT + C_jT\ln T + D_jT^2 + E_jT^{-1} \tag{6} $$

Where A_j, B_j, C_j, D_j and E_j are model parameters to be optimized. Usually A_j and B_j are enough. But in order to fit the heat capacity, at least C_0, D_0, E_0 of the BCC_A2 phase should be of non-zero.

Table 2
Thermodynamic parameters of the U–Mo binary system and U–Mo–Al ternary system obtained in this work.

Phase	Thermodynamic parameters	Reference
Liquid model: $(Al,Mo,U)_1$	${}^{(0)}L^{Liq}_{Mo,U} = -46393.55 + 26.1448 * T$	This work
	${}^{(1)}L^{Liq}_{Mo,U} = -2606.06 + 1.7078 * T$	This work
	${}^{(0)}L^{Liq}_{Al,Mo} = -96235.7 + 20.9416 * T$	[21]
	${}^{(1)}L^{Liq}_{Al,Mo} = -4384.1 + 12.3636 * T$	[21]
	${}^{(2)}L^{Liq}_{Al,Mo} = -25091.6$	[21]
	${}^{(0)}L^{Liq}_{Al,U} = -42716 + 12.376 * T$	[23]
	${}^{(1)}L^{Liq}_{Al,U} = -66098 + 20.347 * T$	[23]
	${}^{(2)}L^{Liq}_{Al,U} = -5000 - 8.656 * T$	[23]
BCC_A2 Model: $(Al,Mo,U)_1:(Va)_3$	${}^{(0)}L^{BCC}_{Mo,U} = 28739.2 - 217.1736 * T + 27.7696 * T * LN(T) + 6.8435E-03 * T^2 - 785719.805 * T^{-1}$	This work
	${}^{(1)}L^{BCC}_{Mo,U} = 27365.2138 - 5.7719 * T$	This work
	${}^{(2)}L^{BCC}_{Mo,U} = 20317.698 - 3.1805 * T$	This work
	${}^{(0)}L^{BCC}_{Al,Mo} = -75938.8 + 10.8187 * T$	[21]
	${}^{(1)}L^{BCC}_{Al,Mo} = -44502.8 + 21.6488 * T$	[21]
	${}^{(2)}L^{BCC}_{Al,Mo} = -22927.1$	[21]
	${}^{(0)}L^{BCC}_{Al,U} = -19,247 + 6.023 * T$	[23]
	${}^{(0)}L^{BCC}_{Al,Mo,U} = -180,000$	This work
	${}^{(1)}L^{BCC}_{Al,Mo,U} = -180,000$	This work
FCC_A1 Model: $(Al,Mo,U)_1:(Va)_1$	${}^{(0)}L^{FCC}_{Al,Mo} = -85,300 + 20.4 * T$	[21]
	${}^{(1)}L^{FCC}_{Al,Mo} = -10,000$	[21]
ort_A20 Model: $(Al,Mo,U)_1$	$G^{ort\_A20}_{Mo} = 21482.5454 + GHSERMO$	This work
	$G^{ort\_A20}_{Al} = 15,000 + GHSERAL$	[23]
	${}^{(0)}L^{ort\_A20}_{Mo,U} = -33595.3252 + 28.2996 * T$	This work
tetr_U Model: $(Al,Mo,U)_1$	$G^{tetr\_U}_{Mo} = 19751.2267 + GHSERMO$	This work
	$G^{tetr\_U}_{Al} = 15,000 + GHSERAL$	[23]
	${}^{(0)}L^{tetr\_U}_{Mo,U} = -12520.8 + 3.5016 * T$	This work
	${}^{(0)}L^{tetr\_U}_{Al,U} = 12,438 - 23.626 * T$	[23]
UAl_2 Model: $(U)_{0.333}:(Al,Mo)_{0.667}$	$G^{UAl_2}_{U:Al} = -32966.7 + 3.4167 * T + 0.667 * GHSERAL + 0.333 * GHSERUU$	[23]
	$G^{UAl_2}_{U:Mo} = 10,000 + 0.333 * GHSERUU + 0.667 * GHSERMO$	This work
	${}^{(0)}L^{UAl_2}_{U:Al,Mo} = -39621.9875 - 1.75 * T$	This work
Laves_C14 Model: $(Al,Mo,U)_{0.333}:(Al,Mo,U)_{0.667}$	$G^{Laves\_C14}_{U:Al} = -19695.1375 - 0.75 * T + 0.333 * GHSERUU + 0.667 * GHSERAL$	This work
	$G^{Laves\_C14}_{U:Mo} = 48,400 - 2.9 * T + 0.333 * GHSERUU + 0.667 * GHSERMO$	This work
	$G^{Laves\_C14}_{U:U} = 50,000 + GHSERUU$	This work
	$G^{Laves\_C14}_{Al:U} = 50,000 + 0.333 * GHSERAL + 0.667 * GHSERUU$	This work
	$G^{Laves\_C14}_{Al:Al} = 50,000 + GHSERAL$	This work
	$G^{Laves\_C14}_{Al:Mo} = 50,000 + 0.333 * GHSERAL + 0.667 * GHSERMO$	This work
	$G^{Laves\_C14}_{Mo:Al} = 50,000 + 0.333 * GHSERMO + 0.667 * GHSERAL$	This work
	$G^{Laves\_C14}_{Mo:U} = 50,000 + 0.333 * GHSERMO + 0.667 * GHSERUU$	This work
	$G^{Laves\_C14}_{Mo:Mo} = 50,000 + GHSERMO$	This work
	${}^{(0)}L^{Laves\_C14}_{U:Al,U} = {}^{(0)}L^{Laves\_C14}_{U:Mo,U} = {}^{(0)}L^{Laves\_C14}_{Al:Al,U} = {}^{(0)}L^{Laves\_C14}_{Al:Mo,U} = {}^{(0)}L^{Laves\_C14}_{Mo:Al,U} = {}^{(0)}L^{Laves\_C14}_{Mo:Mo,U} = {}^{(0)}L^{Laves\_C14}_{Al,U:U} = {}^{(0)}L^{Laves\_C14}_{Mo,U:U} = {}^{(0)}L^{Laves\_C14}_{AL,U:Mo} = {}^{(0)}L^{Laves\_C14}_{Mo,U:Mo} = {}^{(0)}L^{Laves\_C14}_{Al,U:Al} = {}^{(0)}L^{Laves\_C14}_{Mo,U:Al} = 5000$	This work
	${}^{(0)}L^{Laves\_C14}_{Al,Mo:U} = {}^{(0)}L^{Laves\_C14}_{Al,Mo:Mo} = {}^{(0)}L^{Laves\_C14}_{Al,Mo:Al} = 20,000$	This work
	${}^{(0)}L^{Laves\_C14}_{U:Al,Mo} = {}^{(0)}L^{Laves\_C14}_{Mo:Al,Mo} = {}^{(0)}L^{Laves\_C14}_{Al:Al,Mo} = -138,500 + 14.6 * T$	This work
UMo_2Al_{20} Model: $(U)_{0.043}:(Al,Mo)_{0.174}:(Al)_{0.783}$	$G^{UMo_2Al_{20}}_{U:Al:Al} = 7182.875 - 2.5 * T + 0.043 * GHSERUU + 0.957 * GHSERAL$	This work
	$G^{UMo_2Al_{20}}_{U:Mo:Al} = -10,000 + 0.043 * GHSERUU + 0.174 * GHSERMO + 0.783 * GHSERAL$	This work
	${}^{(0)}L^{UMo_2AL_{20}}_{U:Al,Mo:Al} = -88414.375 + 12.5 * T$	This work
$U_6Mo_4Al_{43}$ Model: $(U)_{0.113}:(Al,Mo)_{0.113}:(Al,Mo)_{0.208}:(Al)_{0.566}$	$G^{U_6Mo_4Al_{43}}_{U:Al:Al:Al} = -2663.425 - 0.5 * T + 0.113 * GHSERUU + 0.887 * GHSERAL$	This work
	$G^{U_6Mo_4Al_{43}}_{U:Mo:Al:Al} = -29,000 + 0.113 * GHSERUU + 0.113 * GHSERMO + 0.774 * GHSERAL$	This work
	$G^{U_6Mo_4Al_{43}}_{U:Al:Mo:Al} = -243.125 + 37.5 * T + 0.113 * GHSERUU + 0.208 * GHSERMO + 0.679 * GHSERAL$	This work
	$G^{U_6Mo_4Al_{43}}_{U:Mo:Mo:Al} = 36585.625 + 12.5 * T + 0.113 * GHSERUU + 0.321 * GHSERMO + 0.566 * GHSERAL$	This work
	${}^{(0)}L^{U_6Mo_4Al_{43}}_{U:Al,Mo:Al:Al} = {}^{(0)}L^{U_6Mo_4Al_{43}}_{U:Al,Mo:Mo:Al} = -43414.375 + 12.5 * T$	This work
	${}^{(0)}L^{U_6Mo_4Al_{43}}_{U:Al:Al,Mo:Al} = {}^{(0)}L^{U_6Mo_4Al_{43}}_{U:Mo:Al,Mo:Al} = -111828.75 + 25 * T$	This work
Al_3U Model: $(Al)_{0.75}:(U)_{0.25}$	$G^{Al_3U}_{Al:U} = -31475.0 + 4.5663 * T + 0.75 * GHSERAL + 0.25 * GHSERUU$	[23]
Al_4U Model: $(Al)_{0.8}:(U)_{0.2}$	$G^{Al_4U}_{Al:U} = -25,275 + 3.5022 * T + 0.8 * GHSERAL + 0.2 * GHSERUU$	This work
MoU_2 Model: $(Mo)_{0.333}:(U)_{0.667}$	$G^{MoU_2}_{Mo:U} = -6351.66 + 9.3906 * T - 0.9 * T * LN(T) + 0.333 * GHSERMO + 0.667 * GHSERUU$	This work

Table 2 (*continued*)

Phase	Thermodynamic parameters	Reference
$Al_{12}Mo$ Model: $(Al)_{12}$:$(Mo)_1$	$G^{Al_{12}Mo}_{Al:Mo} = -146766.8 + 23.1256 * T + 12 * GHSERAL + GHSERMO$	[21]
Al_5Mo Model: $(Al)_5$:$(Mo)_1$	$G^{Al_5Mo}_{Al:Mo} = -144819.3 + 25.4357 * T + 5 * GHSERAL + GHSERMO$	[21]
$Al_{22}Mo_5$ Model: $(Al)_{22}$:$(Mo)_5$	$G^{Al_{22}Mo_5}_{Al:Mo} = -723273.3 + 132.3154 * T + 22 * GHSERAL + 5 * GHSERMO$	[21]
$Al_{17}Mo_4$ Model: $(Al)_{17}$:$(Mo)_4$	$G^{Al_{17}Mo_4}_{Al:Mo} = -578455.4 + 107.4145 * T + 17 * GHSERAL + 4 * GHSERMO$	[21]
Al_4Mo Model: $(Al)_4$:$(Mo)_1$	$G^{Al_4Mo}_{Al:Mo} = -138851.8 + 23.1120 * T + 4 * GHSERAL + GHSERMO$	[21]
Al_3Mo Model: $(Al)_3$:$(Mo)_1$	$G^{Al_3Mo}_{Al:Mo} = -143196.7 + 30.6912 * T + 3 * GHSERAL + GHSERMO$	[21]
Al_8Mo_3 Model: $(Al)_8$:$(Mo)_3$	$G^{Al_8Mo_3}_{Al:Mo} = -432556.9 + 99.1737 * T + 8 * GHSERAL + 3 * GHSERMO$	[21]
$Al_{63}Mo_{37}$ Model: $(Al)_{63}$:$(Mo)_{37}$	$G^{Al_{63}Mo_{37}}_{Al:Mo} = -1638310.2 - 403.7604 * T + 63 * GHSERAL + 37 * GHSERMO$	[21]
$AlMo_3$ Model: $(Al,Mo)_1$:$(Al,Mo)_3$	$G^{AlMo_3}_{Al:Mo} = -95830.9 + 2.0081 * T + GHSERAL + 3 * GHSERMO$	[21]
	$G^{AlMo_3}_{Mo:Al} = 135830.9 - 2.0081 * T + 3 * GHSERAL + GHSERMO$	[21]
	$G^{AlMo_3}_{Al:Al} = 20,000 + 4 * GHSERAL$	[21]
	$G^{AlMo_3}_{Mo:Mo} = 20,000 + 4 * GHSERMO$	[21]
	${}^{(0)}L^{AlMo_3}_{Al,Mo:Al} = {}^{(0)}L^{AlMo_3}_{Al,Mo:Mo} = 11628.1$	[21]
	${}^{(0)}L^{AlMo_3}_{Al:Al,Mo} = {}^{(0)}L^{AlMo_3}_{Mo:Al,Mo} = 52,100$	[21]

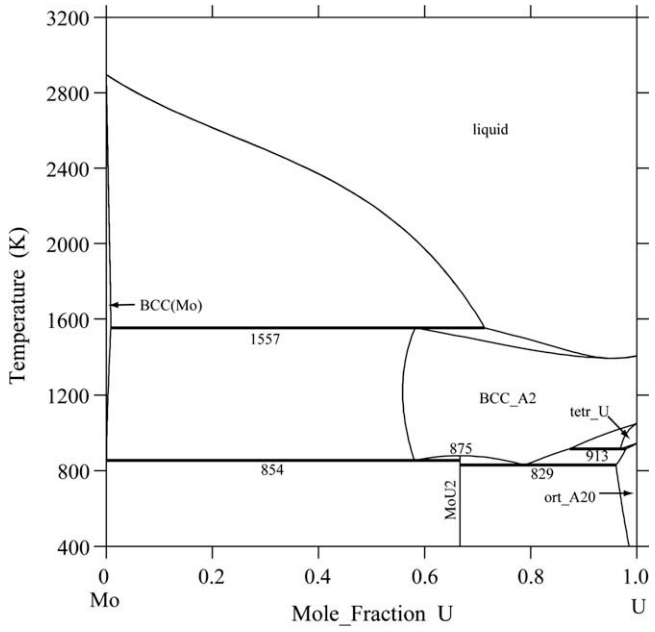

Fig. 3. The calculated U–Mo binary phase diagram in this work.

3.3. Binary intermetallic compounds

Most of the binary intermetallic phases are treated as stoichiometric phases, which are described as M_xN_y. For compounds with no measured heat capacity the formation heat capacity of the compound is assumed to be zero. Then the Kopp–Neumann rule is usually applied to express the Gibbs energy, i.e.

$$G_{M_xN_y} = \frac{x}{x+y}{}^0G^{HSER}_M + \frac{y}{x+y}{}^0G^{HSER}_N + A + BT + CT\ln(T) \quad (7)$$

where M and N denote U, Mo and Al. And A, B and C are the adjusted parameters to be optimized.

Because the homogeneous range of the compound U_2Mo is rather limited, the compound U_2Mo is treated as a stoichiometric phase in order to simplify the assessment.

According to Ref. [25], the UAl_2 phases exhibit ternary solubility of Mo in the U–Mo–Al ternary system. In light of the experimental homogeneity range [25], UAl_2 is modeled as $U_{0.333}$:$(Al,Mo)_{0.667}$, of which the Gibbs energy is formalized as

$$G^{UAl_2} = Y^{II}_{Al}G^{UAl_2}_{U:Al} + Y^{II}_{Mo}G^{UAl_2}_{U:Mo} + 0.667RT\left(Y^{II}_{Al}\ln Y^{II}_{Al} + Y^{II}_{Mo}\ln Y^{II}_{Mo}\right) + Y^{II}_{Al}Y^{II}_{Mo}L^{UAl_2}_{U:Al,Mo} \quad (8)$$

where the superscript II denotes the second sublattice. Y^{II}_{Al} and Y^{II}_{Mo} stand for the site fractions of Al and Mo in the second sublattice, respectively. And the term $L^{UAl_2}_{U:Al,Mo}$ is expressed by the Redlich–Kister polynomials $\sum_{j=0,1\ldots}{}^{(j)}L_{:U:Al,Mo}\left(Y^{II}_{Al} - Y^{II}_{Mo}\right)^j$, representing the interaction between the Al and Mo in the second sublattice in UAl_2. The parameter $G^{UAl_2}_{U:Al}$ is the Gibbs energy of formation of the compound UAl_2, which can be taken from the assessed U–Al binary system [23], and $G^{UAl_2}_{U:Mo}$, the Gibbs energy of the assumed UMo_2 compound with UAl_2 structure, is expressed as

$$G^{UAl_2}_{U:Mo} = 0.333{}^0G^{ort\_A20}_U + 0.667{}^0G^{BCC}_{Mo} + D + ET \quad (9)$$

Here D and E are constants to be optimized in the present work.

3.4. Ternary intermetallic compounds

In this ternary system, the crystal structure refinements and site occupation of atoms of the ternary phases $UMo_{2-x}Al_{20+x}$ and $U_6Mo_{4+x}Al_{43-x}$ have been experimentally investigated by Noël et al. [25]. According to Noël et al. [25], the two phases are described with different models.

The UMo_2Al_{20} phase is described with a three-sublattice model, $(U)_{0.043}$:$(Al,Mo)_{0.174}$:$(Al)_{0.783}$. The Gibbs energy is expressed as

$$G^{UMo_2Al_{20}} = Y^{II}_{Al}G^{UMo_2Al_{20}}_{U:Al:Al} + Y^{II}_{Mo}G^{UMo_2Al_{20}}_{U:Mo:Al} + 0.174RT\left(Y^{II}_{Al}\ln Y^{II}_{Al} + Y^{II}_{Mo}\ln Y^{II}_{Mo}\right) + Y^{II}_{Al}Y^{II}_{Mo} \times \sum_{j=0,1\ldots}{}^{(j)}L^{UMo_2Al_{20}}_{U:Al,Mo:Al}\left(Y^{II}_{Al} - Y^{II}_{Mo}\right)^j \quad (10)$$

where the superscript II denotes the second sublattice. Y^{II}_{Al} and Y^{II}_{Mo} stand for the site fractions of Al and Mo in the second sublattice, respectively. And the term $L^{UMo_2Al_{20}}_{U:Al,Mo:Al}$ represents the interaction between the Al and Mo in the second sublattice in the UMo_2Al_{20}

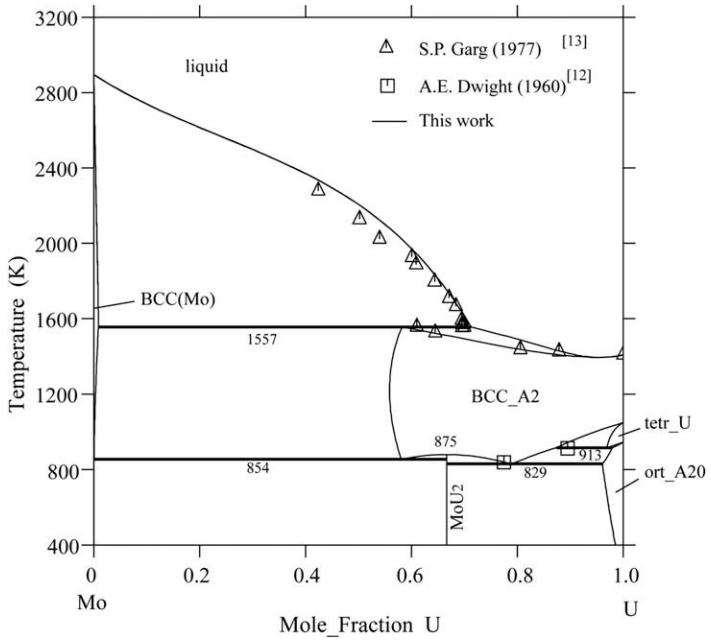

Fig. 4. The assessed phase diagram of the U–Mo binary system in comparison with experiment data.

Table 3
Invariant reactions in the U–Mo binary system.

Invariant reaction	Type	T (K)	Composition (at.% Mo)			Reference
$L + Mo \Longleftrightarrow BCC\_A2$	Peritectic	1557	30.0	39.0	–	[13]
		1557	28.7	41.8	99.1	This work
$BCC\_A2 \Longleftrightarrow Mo + MoU_2$	Eutectoid	853	33.3	–	–	[10]
		854	33.3	41.9	99.9	This work
$BCC\_A2 \Longleftrightarrow MoU_2 + ort\_A20$	Eutectoid	838	–	22.5	–	[12]
		829	3.9	21.1	33.3	This work
$tetr\_U \Longleftrightarrow BCC\_A2 + ort\_A20$	Eutectoid	912	–	–	10.5	[12]
		913	2.1	3.1	12.6	This work
$MoU_2 \Longleftrightarrow BCC\_A2$	Congruent transformation	875	33.3	–	–	[15]
		875	33.3	–	–	This work

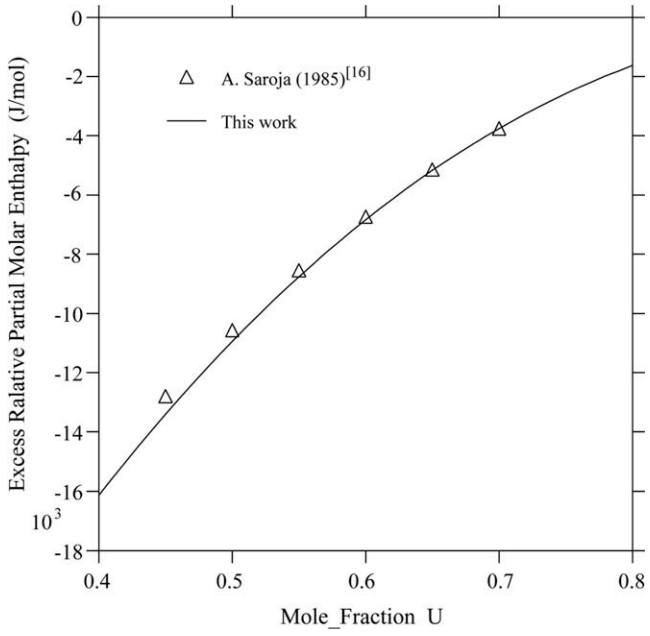

Fig. 5. Comparison of the calculated excess relative partial molar enthalpy of U in liquid U–Mo alloys with the data reported by Saroja et al. [16].

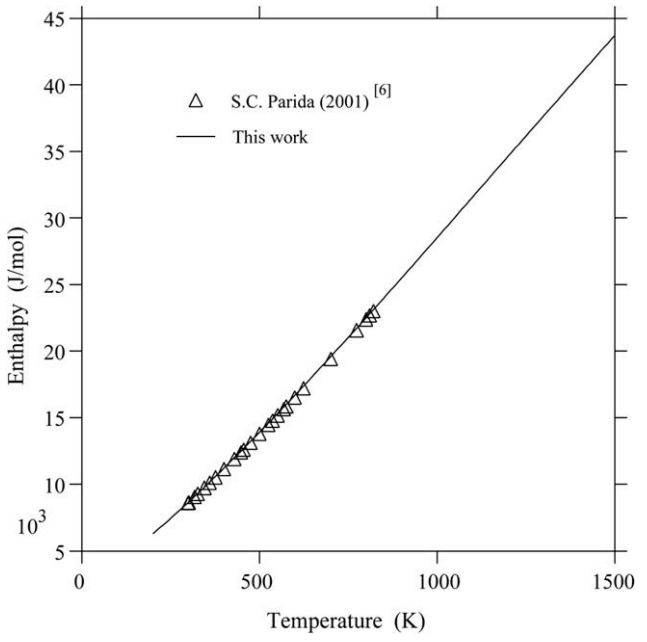

Fig. 6. The assessed variation of enthalpy as a function of temperature for the metastable γ-$U_{0.823}Mo_{0.177}$ in the temperature range 299.0–820.6 K compared with the experiment data [6].

phase. The parameters $G^{UMo_2Al_{20}}_{U:Al:Al}$ and $G^{UMo_2Al_{20}}_{U:Mo:Al}$ are the Gibbs energies of formation of the hypothetical compounds $U_{0.043}Al_{0.957}$ and $U_{0.043}Mo_{0.174}Al_{0.783}$ respectively, which can be calculated as

$$G_{U:Al:Al} = 0.043^0G_U^{ort\_A20} + 0.957^0G_{Al}^{FCC} + J + KT \quad (11)$$

$$G_{U:Mo:Al} = 0.043^0G_U^{ort\_A20} + 0.174^0G_{Mo}^{BCC} + 0.783^0G_{Al}^{FCC} + P + QT \quad (12)$$

where J, K, P and Q are to be assessed.

A four-sublattice model, $(U)_{0.113}$:$(Al,Mo)_{0.113}$:$(Al,Mo)_{0.208}$:$(Al)_{0.566}$, is adopted to model the $U_6Mo_4Al_{43}$ phase. So its Gibbs energy is formalized as

$$\begin{aligned} G^{U_6Mo_4Al_{43}} = {} & Y^{II}_{Al}Y^{III}_{Al}G^{U_6Mo_4Al_{43}}_{U:Al:Al:Al} + Y^{II}_{Al}Y^{III}_{Mo}G^{U_6Mo_4Al_{43}}_{U:Al:Mo:Al} \\ & + Y^{II}_{Mo}Y^{III}_{Al}G^{U_6Mo_4Al_{43}}_{U:Mo:Al:Al} + Y^{II}_{Mo}Y^{III}_{Mo}G^{U_6Mo_4Al_{43}}_{U:Mo:Mo:Al} \\ & + 0.113RT\left(Y^{II}_{Al}\ln Y^{II}_{Al} + Y^{II}_{Mo}\ln Y^{II}_{Mo}\right) \\ & + 0.208RT\left(Y^{III}_{Al}\ln Y^{III}_{Al} + Y^{III}_{Mo}\ln Y^{III}_{Mo}\right) + Y^{II}_{Al}Y^{II}_{Mo}Y^{III}_{Al} \\ & \times \sum_j {}^{(j)}L_{U:Al,Mo:Al:Al}\left(Y^{II}_{Al} - Y^{II}_{Mo}\right)^j + Y^{II}_{Al}Y^{II}_{Mo}Y^{III}_{Mo} \\ & \times \sum_j {}^{(j)}L_{U:Al,Mo:Mo:Al}\left(Y^{II}_{Al} - Y^{II}_{Mo}\right)^j + Y^{II}_{Al}Y^{III}_{Al}Y^{III}_{Mo} \\ & \times \sum_j {}^{(j)}L_{U:Al:Al,Mo:Al}\left(Y^{III}_{Al} - Y^{III}_{Mo}\right)^j + Y^{II}_{Mo}Y^{III}_{Al}Y^{III}_{Mo} \\ & \times \sum_j {}^{(j)}L_{U:Mo:Al,Mo:Al}\left(Y^{III}_{Al} - Y^{III}_{Mo}\right)^j \end{aligned} \quad (13)$$

where Y^{II}_* and Y^{III}_* are the site fractions of Al or Mo in the second and the third sublattices, respectively; $G_{U:*:*:Al}$ represents the Gibbs energies of four hypothetical compounds. ${}^{(j)}L_{U:*:Al,Mo:Al}$ and ${}^{(j)}L_{U:Al,Mo:*:Al}$ represent the jth interaction parameters between the elements Al and Mo in the second and the third sublattices, respectively.

The ternary $UAl_{2-x}Mo_x$ phase takes C14 laves structure and is treated with two sublattices, $(U,Al,Mo)_{0.333}$:$(U,Al,Mo)_{0.667}$. So, its Gibbs energy is formalized as

$$\begin{aligned} G^{UAl_{2-x}Mo_x} = {} & \sum_i\sum_j Y^I_iY^{II}_jG^{UAl_{2-x}Mo_x}_{i:j} \\ & + 0.333RT\left(Y^I_{Al}\ln Y^I_{Al} + Y^I_{Mo}\ln Y^I_{Mo} + Y^I_U\ln Y^I_U\right) \\ & + 0.667RT\left(Y^{II}_{Al}\ln Y^{II}_{Al} + Y^{II}_{Mo}\ln Y^{II}_{Mo} + Y^{II}_U\ln Y^{II}_U\right) \\ & + \sum_i\sum_j\sum_k Y^I_iY^I_jY^{II}_k\sum_{v=0,1,\ldots} {}^{(v)}L_{i,j:k}\left(Y^I_i - Y^I_j\right)^v \\ & + \sum_i\sum_j\sum_k Y^I_kY^{II}_iY^{II}_j\sum_{v=0,1,\ldots} {}^{(v)}L_{k:i,j}\left(Y^{II}_i - Y^{II}_j\right)^v \end{aligned} \quad (14)$$

where i, j, k denote Al, Mo, U, $G^{UAl_{2-x}Mo_x}_{i:j}$ represents the Gibbs energy of nine hypothetical compounds. ${}^{(v)}L_{i,j:j}$ and ${}^{(v)}L_{k:i,j}$ stand for the

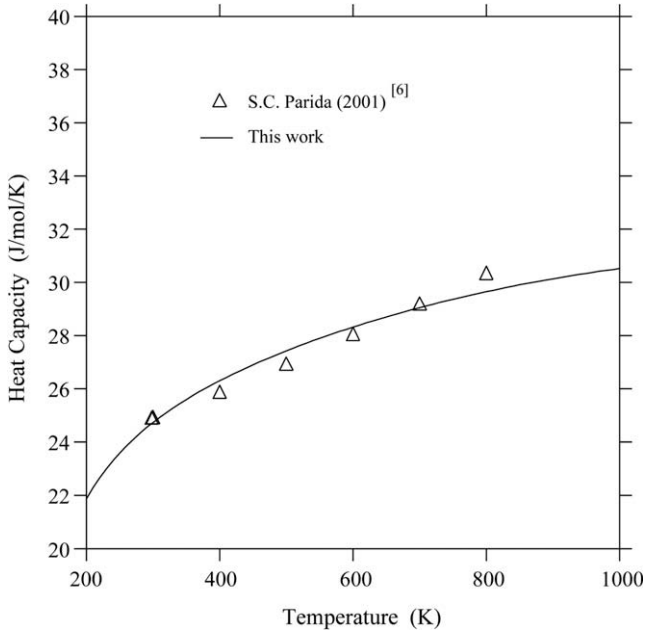

Fig. 7. The calculated heat capacity for the metastable γ-$U_{0.823}Mo_{0.177}$ in comparison with the data reported by Parida et al. [6].

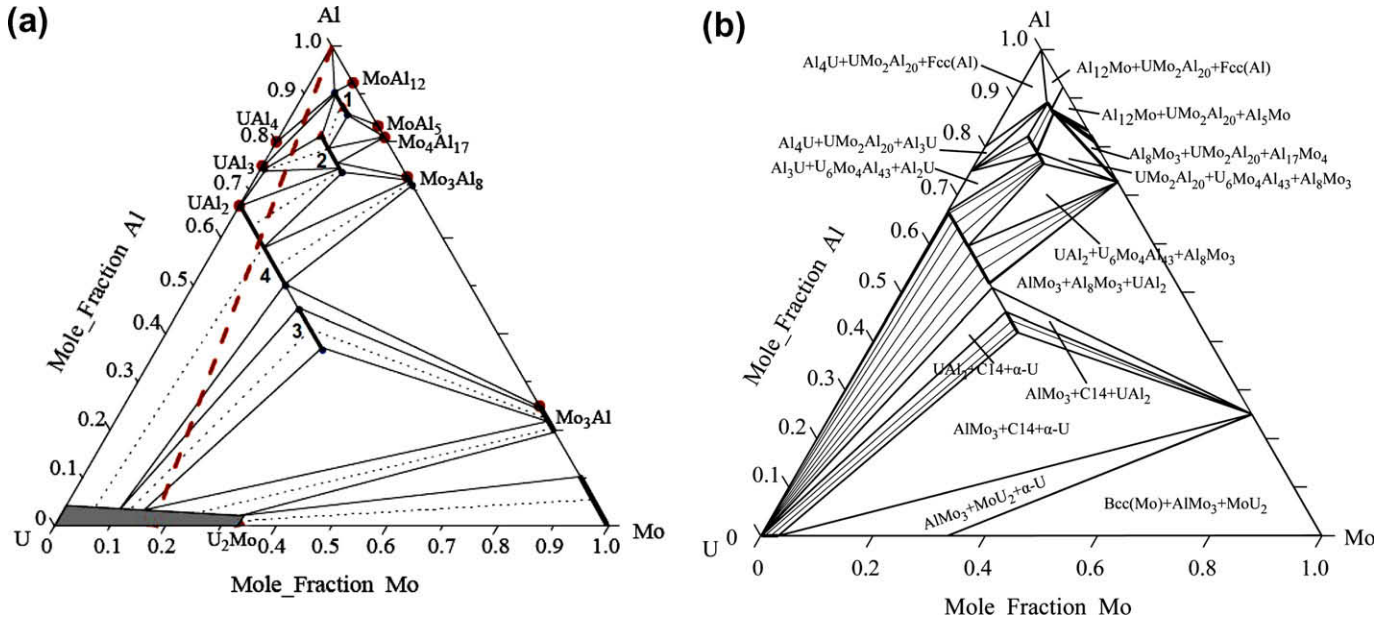

Fig. 8. The isothermal section of U–Mo–Al ternary system at 673 K. (a) Measured by Noël et al. [25], (b) calculated in this work.

interaction parameters between the *i* and *j* in the first (or second) sublattice while the second (or first) sublattice is fully occupied by the element *k*.

4. Results and discussion

4.1. The U–Mo binary system

By adopting the lattice stabilities from Dinsdale [30], and on the basis of phase diagram and reported thermodynamic data, the U–Mo binary system was optimized by using the PARROT module of the Thermo-Calc software package developed by Sundman et al. [31]. After all the experimental data on the phase diagrams and thermodynamic properties were introduced in the program, each of selected data was given a certain weight by personal judgment and varied by trial and error method during the whole assessment until most experimental data were reproduced within the expected uncertainty limits. All of the parameters acquired in present work are listed in Table 2.

The phase diagram calculated in the present work is shown in Fig. 3, and comparison with experimental data reported by Dwight [12], Ackermann and Garg [13] is illustrated in Fig. 4. Especially, experimental and assessed invariant reactions in the U–Mo binary system are further compared as listed in Table 3. It is now clear that except the solubility of U in Mo, most of the reported experimental data were reasonably reproduced. The solubility of U in Mo seems to be smaller than that proposed in Ref. [10]. For the lack of experimental data about the solubility of U in Mo, this difference is

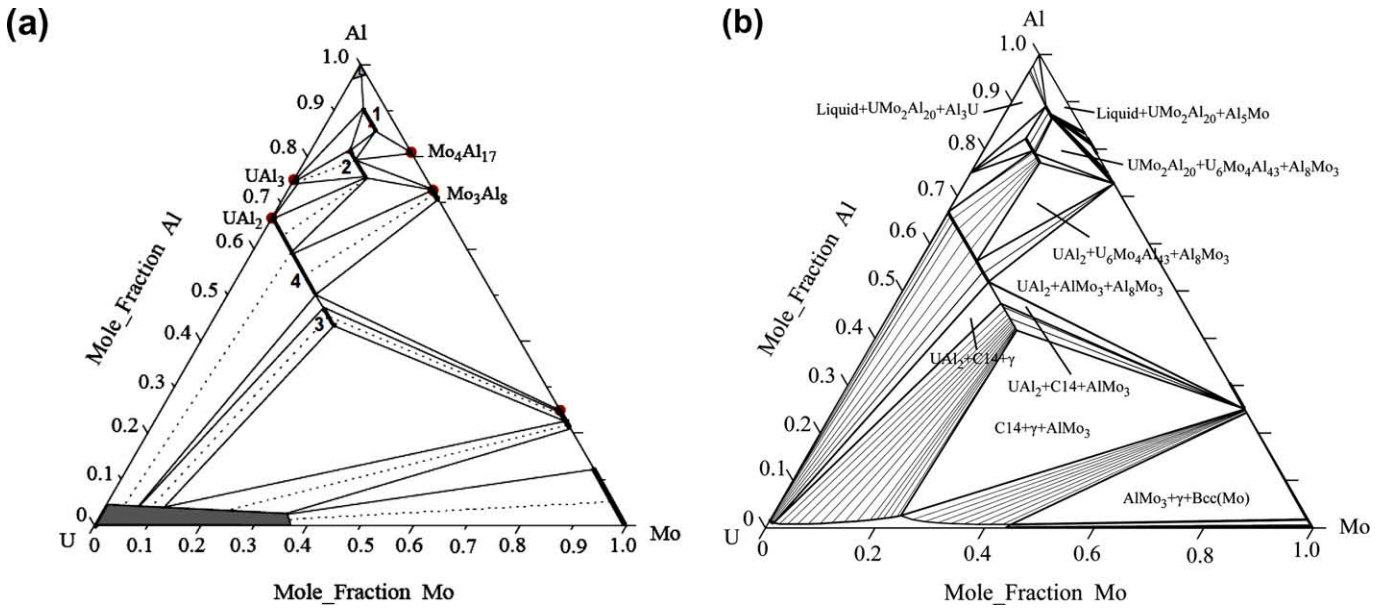

Fig. 9. The isothermal section of U–Mo–Al ternary system at 1073 K. (a) Measured by Noël et al. [25], (b) calculated in this work.

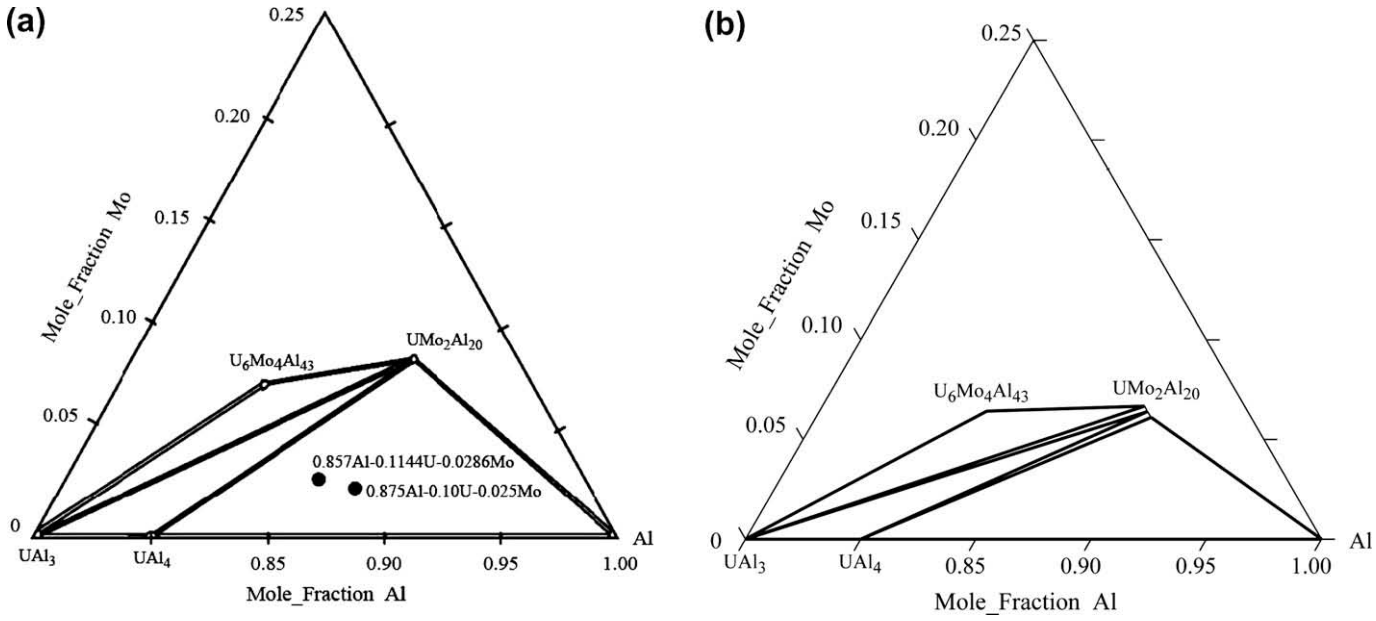

Fig. 10. The partial phase relations of the Al-rich region at 773 K. (a) Measured by Perez et al. [26], (b) calculated in this work.

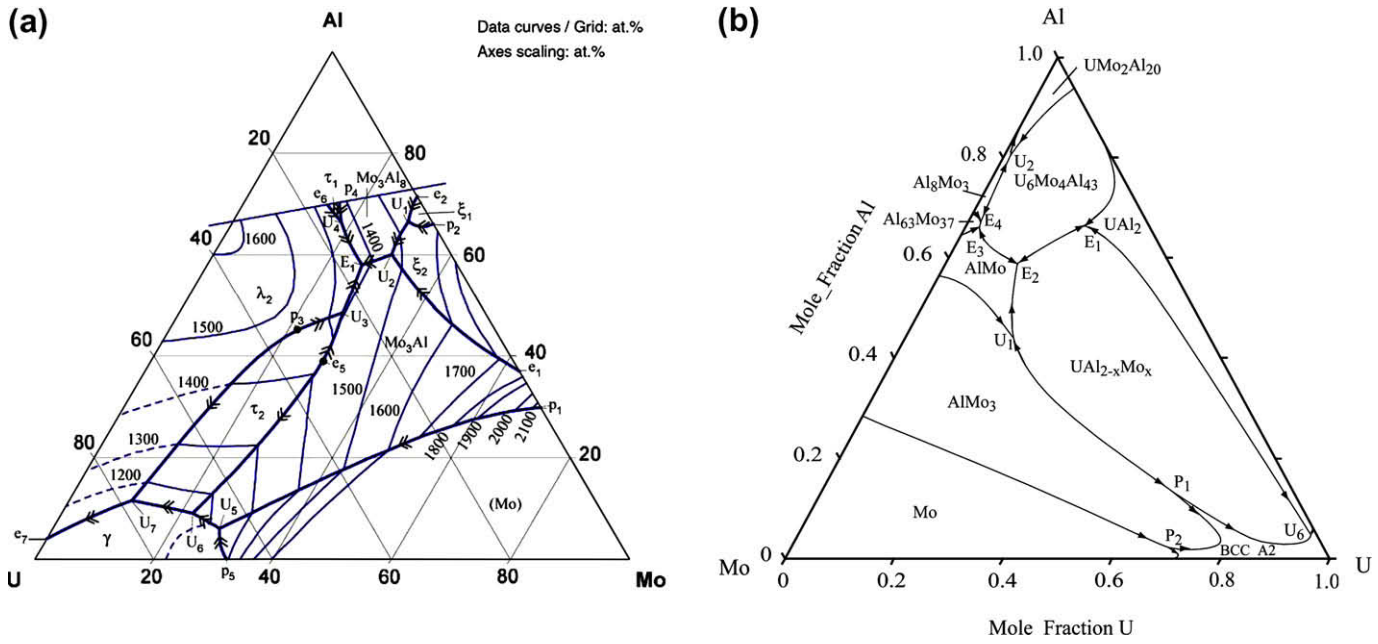

Fig. 11. The liquidus projection of the U–Mo–Al ternary system. (a) Reported by Alekseeva and Korniyenko [29], (b) calculated in this work.

acceptable. On the whole, a good agreement is approached between the calculated and experimental data.

Fig. 5 illustrates the assessed excess relative partial molar enthalpy of liquid of U compared with the data calculated by Saroja et al. [16]. It is shown that good agreement between the assessed value and experimental data is obtained. The variation of enthalpy as a function of temperature for the metastable γ-$U_{0.823}Mo_{0.177}$ in the temperature range 299.0–820.6 K is consistent with the experimental data reported by Parida et al. [6] as demonstrated in Fig. 6. The heat capacity, $C^{o}_{p,m}(T)$, of $U_{0.823}Mo_{0.177}$ alloy was calculated as shown in Fig. 7. Obviously, a very good agreement was realized between this work and the information reported by Parida et al. [6]. So far, it is demonstrated that the experimental thermodynamic data can be well reproduced by the present calculation.

4.2. The U–Mo–Al ternary system

By using the presently optimized parameters of the U–Mo system along with the reported parameters of the Al–Mo [21] and Al–U [23] systems, and based on the detected ternary phase relations, the U–Mo–Al ternary system is further assessed. The optimized parameters are also listed in Table 2.

The experimental and calculated isothermal sections at 673 K and 1073 K for the U–Mo–Al system are shown in Figs. 8 and 9, respectively. The experimental and calculated partial phase diagram of the Al-rich region at 773 K are shown in Fig. 10. It is easy to see that most of the phase relations have been well reproduced.

Certainly, there are some differences between the calculated isothermal sections and the experimental ones [25], e.g. the terminal U-rich BCC_A2 single phase region disappears from the calculated isothermal section at 673 K while was reported to be stable in the experimental one [25]. This confliction may result from that in the present work, it is considered that the BCC_A2 phase has transformed to MoU_2 and ort_A20 through the eutectoid reaction BCC_A2⇔MoU_2 + ort_A20 according to [10]. It is necessary to get much more new experimental data to solve this conflict.

Additionally, some of the equilibria with respect to the $U_6Mo_4Al_{43}$ and UMo_2Al_{20} phase are inconsistent with the measured isothermal sections by Noël et al. [25], e.g. in our assessment, at both 673 K and 1073 K, the $Al_{17}Mo_4$ phase is in equilibrium with UMo_2Al_{20} rather than $U_6Mo_4Al_{43}$ reported by Noël et al. [25]. Besides, equilibriums between UMo_2Al_{20} and Al_5Mo, $Al_{22}Mo_5$, Al_3Mo at 1073 K, as well as the equilibrium between UMo_2Al_{20} and $Al_{22}Mo_5$ at 673 K are established in our assessment which were not reported in [25]. These differences are due to the assessed phase diagram of Al–Mo binary system used in this work is relatively new. So this part of the isothermal section needs to be confirmed by more experiments.

The calculated liquidus projection is compared with [29] in Fig. 11 and the calculated invariant reactions and temperatures involved liquid in the U–Mo–Al ternary system are summarized in Table 4. Invariant reactions U_3, U_9, U_{11} and E_5 are very close to the Al–U binary subsystem, and U_4, U_5, U_7, U_8 and U_{10} are very near to the Al–Mo binary subsystem, so these 10 invariant reactions cannot be visible in Fig. 11. Compared to the experimental results [29], there are several different parts, especially the reactions concerning the Al-rich region, including the compounds $U_6Mo_4Al_{43}$

Table 4
Calculated Invariant Reactions and Temperatures of the U–Mo–Al Ternary System.

Type	Reaction	T (K)
E_1	$L \Longleftrightarrow UAl_{2-x}Mo_x + UAl_2 + U_6Mo_4Al_{43}$	1915.6
E_2	$L \Longleftrightarrow U_6Mo_4Al_{43} + AlMo + UAl_2$	1813.4
E_3	$L \Longleftrightarrow U_6Mo_4Al_{43} + Al_{63}Mo_{37} + AlMo$	1790.7
E_4	$L \Longleftrightarrow U_6Mo_4Al_{43} + Al_{63}Mo_{37} + Al_8Mo_3$	1790.3
E_5	$L \Longleftrightarrow Al_4U + FCC\_A1 + UMo_2Al_{20}$	915.4
U_1	$L + AlMo_3 \Longleftrightarrow AlMo + UAl_{2-x}Mo_x$	1966.0
U_2	$L + U_6Mo_4Al_{43} \Longleftrightarrow UMo_2Al_{20} + Al_8Mo_3$	1783.0
U_3	$L + UAl_2 \Longleftrightarrow U_6Mo_4Al_{43} + Al_3U$	1623.9
U_4	$L + Al_8Mo_3 \Longleftrightarrow Al_3Mo + UMo_2Al_{20}$	1498.8
U_5	$L + Al_3Mo \Longleftrightarrow Al_4Mo + UMo_2Al_{20}$	1429.2
U_6	$L + UAl_{2-x}Mo_x \Longleftrightarrow BCC\_A2 + UAL_2$	1384.9
U_7	$L + Al_4Mo \Longleftrightarrow Al_{17}Mo_4 + UMo_2Al_{20}$	1267.7
U_8	$L + Al_{17}Mo4 \Longleftrightarrow Al_{22}Mo_5 + UMo_2Al_{20}$	1221.1
U_9	$L + U_6Mo_4Al_{43} \Longleftrightarrow Al_3U + UMo_2Al_{20}$	1144.7
U_{10}	$L + Al_{22}Mo_5 \Longleftrightarrow Al_5Mo + UMo_2Al_{20}$	1121.4
U_{11}	$L + Al_3U \Longleftrightarrow Al_4U + UMo_2Al_{20}$	1004.3
P_1	$L + UAl_{2-x}Mo_x + AlMo_3 \Longleftrightarrow BCC\_A2$	1720.0
P_2	$L + Mo + AlMo_3 \Longleftrightarrow BCC\_A2$	1662.2

and UMo_2Al_{20}. And the Mo_2Al_3 phase mentioned in [29] is not included in this work according to [21]. In consideration of the lack of new liquid experiment data of the Al-rich region and uncertain parts of the liquidus projection determinated by Petzow and Rexer [28], further experimental information is needed to verify the liquidus projection.

5. Conclusions

During the present calculation, thermodynamic descriptions of the U–Mo binary system and the U–Mo–Al ternary system are developed based on previous phase diagram data and thermodynamic data. Reasonable agreement between calculated and experimental data has been acquired. A set of self-consistent thermodynamic parameters has been constructed to reproduce the U–Mo–Al ternary system.

Acknowledgment

This work was financially supported by China Institute of Atomic Energy, PR China.

References

[1] E.F. Kryuchkov, M.S. Kushnarev, V.B. Glebov, V.A. Apse, A.N. Shmelev, Prog. Nucl. Energy 50 (2008) 643–646.
[2] H.J. Ryu, Y.S. Han, J.M. Park, S.D. Park, C.K. Kim, J. Nucl. Mater. 321 (2003) 210–220.
[3] N. Wieschalla, A. Bergmaier, P. Boni, K. Boning, G. Dollinger, R. Großmann, W. Petry, A. Rohrmoser, J. Schneider, J. Nucl. Mater. 357 (2006) 191–197.
[4] K.H. Kim, J.M. Park, C.K. Kim, G.L. Hofman, M.K. Meyer, Nucl. Eng. Des. 211 (2002) 229–235.
[5] C.G. Yin, Atom. Energy Sci. Technol. 39 (2005) 94–98.
[6] S.C. Parida, S. Dash, Z. Singh, R. Prasad, V. Venugopal, J. Phys. Chem. Solids 62 (2001) 585–597.
[7] J.E. Garces, A.C. Marino, G. Bozzolo, Appl. Surf. Sci. 219 (2003) 47–55.
[8] J.J. Burke, D.A. Colling, A.E. Gorum, J. Greenspan (Eds.), Physical Metallurgy of Uranium Alloys, Proceedings of the Third Army Materials Technology Conference, Brook Hill Publishing Company, 1976.
[9] F. Mazaudier, C. Proye, F. Hodaj, J. Nucl. Mater. 377 (2008) 476–485.
[10] T.B. Massalski (editor-in-chief), Binary Alloy Phase Diagrams, second ed., vol. 3, Materials Information Soc., Materials Park, Ohio, 1990.
[11] Kaufman, H. Bernstein, Computer Calculation of Phase Diagrams, Academic Press, New York, 1970.
[12] A.E. Dwight, J. Nucl. Mater. 2 (1960) 81–87.
[13] R.J. Ackermann, S.P. Garg, J. Nucl. Mater. 64 (1977) 265–274.
[14] M. Hansen, K. Anderko, Constitution of Binary Alloys, 2nd ed., Springer, Berlin, 1958.
[15] L. Brewer, R.H. Lamoreaux, R. Ferro, R. Marazza, K. Girgis, in: Molybdenum: Physico-Chemical Properties of its Compounds and Alloys, in: L. Brewer (Ed.), Atomic Energy Review, 7, IAEA, Vienna, 1980, pp. 336–338 (special issue).
[16] A. Saroja, Y.J. Bhatt, S.P. Garg, J. Less-Common Met. 114 (1985) 291–297.
[17] R. Hultgren, P.D. Desai, D.T. Hawkins, M. Gleiser, K.K. Kelley, D.D. Wagman, Selected Values of Thermodynamic Properties of the Elements, American Society for Metals, Metals Park, OH, 1973.
[18] N. Saunders, J. Phase Equilib. 18 (1997) 370–378.
[19] J.C. Schuster, H. Ipser, Mater. Trans. A 22 (1991) 1729–1736.
[20] M. Eumann, G. Sauthoff, M. Palm, Int. J. Mater. Res. 97 (2006) 1502–1511.
[21] Z.M. Du, C.P. Guo, C.R. Li, W.J. Zhang, J. Phase Equilib. 30 (2009) 487–501.
[22] M.E. Kassner, P.H. Adler, M.G. Adamson, J. Nucl. Mater. 167 (1989) 160.
[23] J. Wang, X.J. Liu, C.P. Wang, J. Nucl. Mater. 374 (2008) 79–86.
[24] Olivier Tougait, Henri Noël, Intermetallics 12 (2004) 219–223.
[25] H. Noël, O. Tougait, S. Dubois, J. Nucl. Mater. 389 (2009) 93–97.
[26] E. Perez, A. Ewh, J. Liu, B. Yuan, D.D. Keiser Jr., Y.H. Sohn, J. Nucl. Mater. 394 (2009) 160–165.
[27] D.D. Keiser Jr., C.R. Clark, M.K. Meyer, Scripta Mater. 51 (2004) 893.
[28] G. Petzow, J. Rexer, Z. Metallkd 60 (5) (1969) 449–453.
[29] Zoya Alekseeva, Kostyantyn Korniyenko (Aluminium–molybdenum–uranium), in: Günter Effenberg, Svitlana Ilyenko (Eds.), SpringerMaterials – The Landolt-Börnstein Database, Springer-Verlag, Berlin, Heidelberg, 2009.
[30] A.T. Dinsdale, CALPHAD 15 (1991) 317–425.
[31] B. Sundman, B. Jansson, J.O. Andersson, CALPHAD 9 (1985) 153–190.